Probing the role of photon strength function models in determining the properties of the hot giant dipole resonance

Debasish Mondal,[1,*] Chandrani Sen,[1,2] S. Mukhopadhyay,[1,2] Deepak Pandit,[1,2] Surajit Pal,[1] J. Sadhukhan,[1,2] Saumanti Sadhukhan,[1,2] Balaram Dey,[3] Srijit Bhattacharya,[4] A. De,[5] Pratap Roy,[1,2] T. K. Rana,[1,2] Rajkumar Santra,[1] and C. Bhattacharya[1,2]

[1]*Variable Energy Cyclotron Centre, 1/AF-Bidhannagar, Kolkata-700064, India*
[2]*Homi Bhabha National Institute, Training School Complex, Anushaktinagar, Mumbai-400094, India*
[3]*Department of Physics, Bankura University, Bankura - 722155, India*
[4]*Department of Physics, Barasat Government College, Barasat, N 24 Pgs, Kolkata - 700124, India*
[5]*Department of Physics, Raniganj Girls' College, Raniganj-713358, India*

(Received 25 October 2023; revised 28 February 2024; accepted 22 April 2024; published 23 May 2024)

Temperature-dependent photon strength function (PSF) models, along with the widely accepted temperature-independent Brink-Axel Lorentzian model, are investigated in their application to determine the properties of the giant dipole resonance (GDR) built on the excited states of nuclei up to a temperature ≈1.5 MeV. Three temperature-dependent models, namely, the simple modified Lorentzian model, the hybrid model by Goriely, and the generalized Lorentzian model of Kopecky and Uhl, are studied. The statistical model calculations with all PSF models reproduce the high-energy ($E_\gamma \approx$ 5–25 MeV) γ-ray spectra originating from the decay of ^{62}Zn and ^{201}Tl compound nuclei reasonably well, and put forward approximately the same peak energy and strength of the GDR. Nevertheless, at a given temperature, significant variation is observed in the predicted GDR width, which may influence the theoretical models used to calculate the GDR width.

DOI: 10.1103/PhysRevC.109.054322

I. INTRODUCTION

The atomic nucleus is a many-body quantum system endowed with various giant resonances, wherein all nucleons participate collectively [1]. The isovector giant dipole resonance (IVGDR or commonly referred to as GDR) is one such resonance perceived macroscopically as an out-of-phase vibration of protons and neutrons within the nucleus. In a microscopic picture, it is described as a coherent superposition of $1p$-$1h$ configurations across one major shell. The GDR built on the ground state has traditionally been studied by photoabsorption reactions. The resonant lineshape is approximately represented by a Lorentzian curve given by [2,3]

$$\sigma_{\mathrm{E1}}(E_\gamma) = \sigma_{\mathrm{TRK}} S_{\mathrm{G0}} \frac{2}{\pi} \frac{\Gamma_{\mathrm{G0}} E_\gamma^2}{\left(E_\gamma^2 - E_{\mathrm{G0}}^2\right)^2 + \Gamma_{\mathrm{G0}}^2 E_\gamma^2}, \qquad (1)$$

where $\sigma_{\mathrm{TRK}} = 60\frac{NZ}{A}$ mb MeV is obtained from the Thomas-Reiche-Kuhn (TRK) dipole sum rule. E_{G0}, Γ_{G0}, and S_{G0} are the GDR energy, width, and the fraction of the TRK sum rule exhausted by the GDR, respectively. The GDR lineshape in Eq. (1) is commonly referred to as the Brink-Axel Lorentzian or the standard Lorentzian (SLO). Conversely, the GDR built on the excited states [4–8] is studied by measuring the γ decay from an excited compound nucleus (CN) which is populated through fusion evaporation reaction [9–16] or by inelastic scattering reaction [17]. Typically, the γ rays in the energy range of $E_\gamma \approx$ 5–30 MeV are measured with large-volume scintillation detectors. The parameters of the GDR are determined by fitting the measured γ-ray spectrum with the result of the statistical model calculation performed traditionally by using the CASCADE code [18], modified to include the γ decay from the GDR. Generally, the γ-decay rate is calculated using the photon strength function (PSF) obtained from the SLO photoabsorption cross section in the inverse channel and is given by

$$f_{E1}(E_\gamma) = K_1 \frac{\sigma_{E1}(E_\gamma)}{E_\gamma}, \qquad (2)$$

where $K_1^{-1} = 3(\pi\hbar c)^2$. The GDR parameters E_{G}, Γ_{G}, and S_{G} are determined by fitting the experimental data. E_{G} (Γ_{G} and S_{G}) is different from E_{G0} (Γ_{G0} and S_{G0}) in the sense that it represents the energy (width and strength) of the GDR built on the excited state of the nucleus. Interestingly, the PSF given by Eq. (2) solely depends on the γ-ray energy, not on the specific properties or absolute energies of the states involved in the transition [19,20], though a few conflicting experimental results have been observed in recent years [21–25]. In a few studies [17,26,27], the PSF is varied along the decay cascade by varying the GDR width. However, in general, the PSF is kept unchanged throughout the decay cascade. It has been also observed that the SLO model [Eq. (1)] overestimates the measured absorption cross sections below the peak of the GDR and underestimates it above the peak [28].

*debasishm@vecc.gov.in

In recent years, the PSF has attracted substantial experimental and theoretical efforts owing to its pivotal role in astrophysical reaction model calculations aimed at understanding elemental abundances in the universe. Notably, the studies performed by using the Oslo method [29–34] are worth mentioning, where the low-energy part of the PSF ($E_\gamma \lessapprox 10$ MeV) is determined together with nuclear level density (NLD). Theoretically, various modified PSFs have been proposed, namely, the generalized Lorentzian model by Kopecky and Uhl (KLO) [35], the hybrid model by Goriely (GLO) [36], the simple modified Lorentzian model (SMLO) [28,37,38], building upon the works of Kadmenskij *et al.* [39] in the framework of the Fermi liquid theory of finite systems. The primary feature of these PSFs is that, they depend on the γ-ray energy as well as the temperature of the state to which the transition occurs. By using the modified PSF, Kopecky and Uhl showed that the thermal neutron capture cross sections substantially improved as compared to the SLO model [35]. Additionally, it seems that the choice of the PSF model significantly affects the elemental abundances in astrophysical reaction models [36]. These temperature-sensitive PSFs may have significant impact on the properties of the GDR built on the excited states of nuclei, as well as, various properties of excited nuclei, namely isospin mixing [40–43], nuclear viscosity [44,45], fission time scale [46–48], etc which are studied by using the γ-decay from the GDR as a probe, and the SLO model is utilized in the analysis of the experimental data.

In a recent study, coordinated by the International Atomic Energy Agency, a reference database for the PSFs has been created from the photoabsorption data, where the parameters of the GDR built on the ground state of the nuclei, have been evaluated both by the SLO and SMLO models [28]. Therefore, it is apparent that the temperature-dependent PSF models, which were primarily proposed to take care of the overestimation of the absorption cross section near the particle threshold by the SLO, warrants exploration at high excitations. In this paper, we report the results of the analyses of the measured high-energy γ-ray spectra for ^{62}Zn and ^{201}Tl with four different prescriptions of the PSF, namely, SLO, KLO, GLO, and SMLO.

II. EXPERIMENTAL DETAILS

^{62}Zn compound nucleus was populated at high excitations by bombarding pulsed ^{4}He-ion beam from the K-130 room-temperature cyclotron at the Variable Energy Cyclotron Centre (VECC), Kolkata, India on self-supporting ^{58}Ni target. The data for ^{201}Tl were taken from an earlier experiment performed at VECC by our group using ^{4}He-ion beam on self-supporting ^{197}Au target [13]. The initial excitation energies (E^*) of ^{201}Tl were 32.8, 39.6, and 47.5 MeV corresponding to the beam energies of 35, 42, and 50 MeV, respectively, whereas, ^{62}Zn was excited at 29.5 and 40.8 MeV with 28 and 40 MeV beam energies, respectively. The high-energy γ rays were detected by using a part of the LAMBDA spectrometer [49]. A total of 49 BaF_2 scintillators, each measuring $3.5 \times 3.5 \times 35$ cm^3, were arranged in a 7×7 matrix configuration which was positioned at a distance of approximately 50 cm from the target, at an angle of approximately 90° with respect to the beam direction. In addition, a low-energy γ-ray multiplicity filter [50] was utilized to determine the angular momentum (J) distribution of the CN population. A total of 50 BaF_2 scintillators each measuring $3.5 \times 3.5 \times 5$ cm^3 were divided into two groups of 25 detectors. Each group was arranged in a 5×5 closed-packed, staggered-castle type geometry and placed on the top and bottom of the target chamber approximately 4.5 cm away from the target position. The master trigger was generated by the triple coincidence of the OR signals from the LAMBDA, top, and bottom multiplicity filters. In each event, the energy and time for each element of the LAMBDA were recorded, along with the number of multiplicity detectors fired (referred to as fold) using a VME-based data acquisition system. The start trigger for time measurement was taken from the multiplicity filters. The time spectrum of the cyclotron radiofrequency was recorded to minimize the random coincidences. The high-energy γ-ray spectra were generated using the cluster summing technique, where cosmic events were rejected by their hit pattern in the LAMBDA array [49]. The neutron and pile-up events were rejected by applying prompt gates in the time-of-flight and pulse shape discrimination (PSD) spectra, respectively, of each element of LAMBDA. The PSD technique was implemented by measuring the charge deposition over two integrating time intervals of approximately 30 ns and 2 μs.

III. STATISTICAL MODEL CALCULATIONS

The GDR parameters were determined from the measured high-energy γ-ray spectra by the statistical model calculations performed within the Hauser-Feshbach formalism with version 1.95 of the TALYS code [51] (TALYS-1.95). The crucial inputs for calculating the γ-ray yield are the angular momentum distribution of the fusion cross section of the initial CN, the γ-ray transmission coefficients, and the NLD. Since the master trigger was generated by taking the top-bottom coincidence of the multiplicity detectors, events with slightly higher angular momentum were selected. Therefore, the CN population was simulated from the measured fold distribution using GEANT3 toolkit. A triangular distribution is utilized as input in the simulation, and the CN population distribution is determined by comparing the measured and simulated fold distributions. As an example, the measured and simulated fold distributions are shown in Fig. 1(a), and the simulated CN population distribution is shown in Fig. 1(b) along with the input distribution. In Figs. 1(c) and 1(d), the simulated CN populations as a function of J are shown at different excitation energies for ^{62}Zn and ^{201}Tl, respectively. The details of the procedure can be found in Ref. [50]. The statistical model calculations have been performed by incorporating these initial populations into the TALYS code. The decay width of a γ-ray of energy E_γ, type X, and multipolarity L is proportional to the transmission coefficient [$T_{XL}(E_\gamma)$] and level density of the final state. The γ-ray transmission coefficient is given by $T_{XL}(E_\gamma) = 2\pi f_{XL}(E_\gamma) E_\gamma^{(2L+1)}$. In the present study, γ rays up to $L = 2$ are considered. However, the γ-ray spectrum is primarily governed by the $E1$ strength function for which four different models, as mentioned earlier, are investigated in

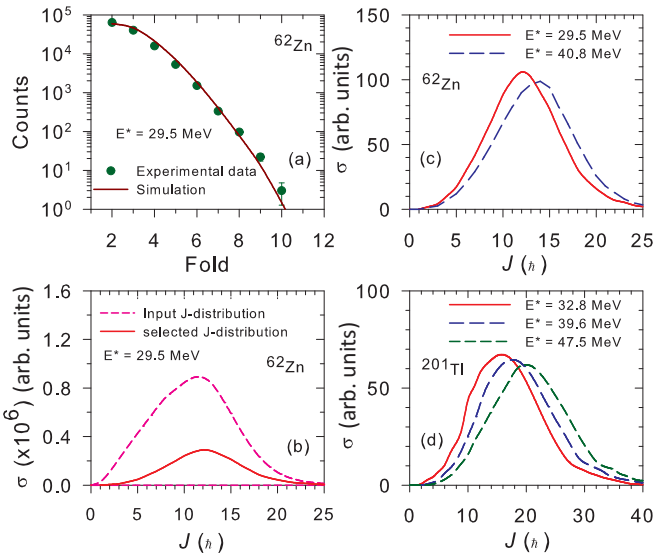

FIG. 1. (a) Measured and simulated fold distributions for ^{62}Zn at $E^* = 29.5$ MeV. (b) Input and selected CN population distribution in the simulation are shown as a function of J for ^{62}Zn at $E^* = 29.5$ MeV. All simulated CN population distributions as a function of J are shown for (c) ^{62}Zn and (d) ^{201}Tl. The areas under the distributions are normalized to 1000.

the present study. The general form of these $E1$ PSFs can be expressed as

$$f_{E1}(E_\gamma, T) = K_1 \sigma_{\mathrm{TRK}} S_{\mathrm{G}} \frac{G\{E_\gamma, E_{\mathrm{G}}, \Gamma(E_\gamma, T)\}}{E_\gamma}, \quad (3)$$

where T is the temperature of the final state. The absorption cross section in the inverse channel can be calculated from Eqs. (2) and (3) as

$$\sigma_{E1}(E_\gamma, T) = \sigma_{\mathrm{TRK}} S_{\mathrm{G}} G\{E_\gamma, E_{\mathrm{G}}, \Gamma(E_\gamma, T)\}. \quad (4)$$

The function $G\{E_\gamma, E_{\mathrm{G}}, \Gamma(E_\gamma, T)\}$ can be expressed in general as

$$G\{E_\gamma, E_{\mathrm{G}}, \Gamma(E_\gamma, T)\} = \frac{2}{\pi} C(E_\gamma, T) \frac{\Gamma(E_\gamma, T) E_\gamma^2}{\left(E_\gamma^2 - E_{\mathrm{G}}^2\right)^2 + \Gamma(E_\gamma, T)^2 E_\gamma^2}. \quad (5)$$

The functions $C(E_\gamma, T)$ and $\Gamma(E_\gamma, T)$ vary for different PSF models, as shown in Table I. In the KLO model, a zero-energy limit of the strength function is added to Eq. (3) (see Eq. (2.4) in Ref [35]). In the GLO model, $\Gamma(E_\gamma, T)^2$ in the denominator of Eq. (5) is replaced by $\Gamma_{\mathrm{G}}\Gamma(E_\gamma, T)$. S_{G} may be considered, by definition, the fraction of the TRK sum rule exhausted by the GDR, if $\int_0^\infty G\{E_\gamma, E_{\mathrm{G}}, \Gamma(E_\gamma, T)\} dE_\gamma = 1$. This holds true for the SLO model. However, for the temperature-dependent PSFs, this is not the case. Therefore, for these models, temperature-dependent corrections are applied to normalize the value of the integration to that obtained for the SLO model in the range of $E_\gamma = 0$–30 MeV. These corrections, however, do not significantly affect the high-energy γ-ray spectra. The fits were achieved by varying the GDR parameters E_{G}, Γ_{G}, and S_{G} [see Eq. (3) and Table I]. In the SLO model, the same value of Γ_{G} was used throughout the decay cascade. However, for the temperature-sensitive PSF models, since the strength is dependent on $\Gamma(E_\gamma, T)$, it varies along the decay cascade. The E_{G} is scaled according to the $A^{-1/3}$ law, relative to the value of the initial CN, for all nuclei in the decay cascade. We remark here that, except for the SLO model, Γ_{G} in Table I should be denoted as Γ_{G0}, because the $\Gamma(E_\gamma, T)$ for these models is originally parameterized in terms of the ground state GDR width. However, since we have utilized it as a free parameter to fit the high-energy γ-ray spectrum, it has been denoted by Γ_{G}.

TABLE I. Expressions of $C(E_\gamma, T)$ and $\Gamma(E_\gamma, T)$ for different models of the PSF.

PSF model	$C(E_\gamma, T)$	$\Gamma(E_\gamma, T)$
SLO	1	Γ_{G}
SMLO	$\frac{1}{1-\exp[-\frac{E_\gamma}{T}]}$	$\frac{\Gamma_{\mathrm{G}}}{E_{\mathrm{G}}}[E_\gamma + \frac{4\pi^2 T^2}{E_{\mathrm{G}}}]$
KLO	1	$\frac{\Gamma_{\mathrm{G}}}{E_{\mathrm{G}}^2}[E_\gamma^2 + 4\pi^2 T^2]$
GLO	1	$0.7\frac{\Gamma_{\mathrm{G}}}{E_{\mathrm{G}}}[E_\gamma + \frac{4\pi^2 T^2}{E_\gamma}]$

Apart from the strength function, the γ-decay width depends on the NLD, as mentioned earlier. In this study, we utilized two phenomenological models, e.g., the back-shifted Fermi gas model (BFM) and the constant temperature model (CTM) as introduced by Gilbert and Cameron [52]. The Fermi gas level density, at an excitation energy E_{x} and angular momentum J, is given by

$$\rho(E_{\mathrm{x}}, J) = \frac{2J+1}{2\sigma^2} \exp\left[-\frac{\left(J+\frac{1}{2}\right)^2}{2\sigma^2}\right] \rho_{\mathrm{f}}^t(E_{\mathrm{x}}), \quad (6)$$

where σ^2 is the spin cut-off parameter and $\rho_{\mathrm{f}}^t(E_{\mathrm{x}})$ is the total Fermi gas level density at excitation energy E_{x} given by

$$\rho_{\mathrm{f}}^t(E_{\mathrm{x}}) = \frac{1}{\sqrt{2\pi}\sigma} \frac{\sqrt{\pi}}{12} \frac{\exp[2\sqrt{a(E_{\mathrm{x}} - \Delta)}]}{a^{\frac{1}{4}}(E_{\mathrm{x}} - \Delta)^{\frac{5}{4}}}, \quad (7)$$

where a is the level density parameter (LDP) and Δ is an empirical parameter closely related to the pairing energy. In the BFM, Eq. (7) is utilized to calculate the total level density for all E_{x}. On the other hand, the total level density up to an energy E_{M} is approximated by a constant temperature formula in the CTM viz.

$$\rho_{\mathrm{CTM}}^t(E_{\mathrm{x}}) = \frac{1}{T_0} \exp\left[\frac{E_{\mathrm{x}} - E_0}{T_0}\right] \quad (8)$$

and above E_{M}, the total level density is calculated by the Fermi gas formula [Eq. (7)]. Within the TALYS code, E_{M}, E_0, and T_0 are determined from the smooth matching of the level densities predicted by the CTM and BFM at $E_{\mathrm{x}} = E_{\mathrm{M}}$, along with the available experimental values of the NLD at low excitation energies. The shell effect is incorporated into the level density parameter by the prescription of Ignatyuk *et al.* and is given by $a(U) = \tilde{a}[1 + \frac{\Delta S}{U}\{1 - \exp(-\gamma U)\}]$ [53], where $U = E_{\mathrm{x}} - \Delta$. ΔS represents the ground state shell correction and γ is the shell damping factor given by $\gamma = \frac{\gamma_1}{A^{1/3}}$. In the TALYS code, the asymptotic level density parameter is

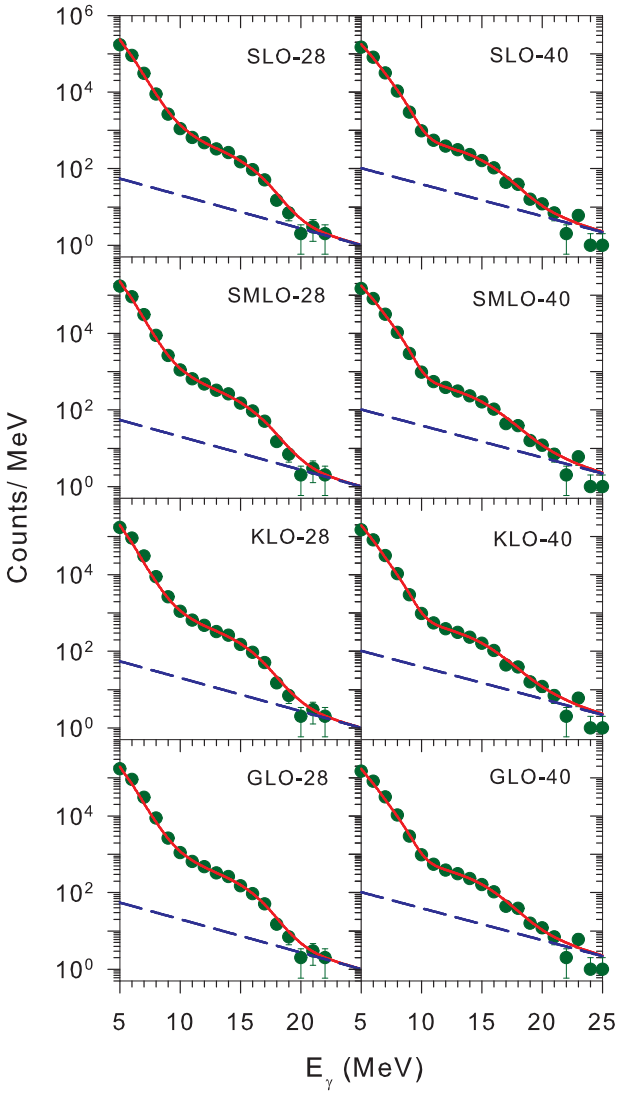

FIG. 2. Experimental high-energy γ-ray spectra (symbols) originated from the decay of ^{62}Zn compound nucleus along with the results (lines) of statistical model calculations with different PSF models. The dashed lines represent the bremsstrahlung component.

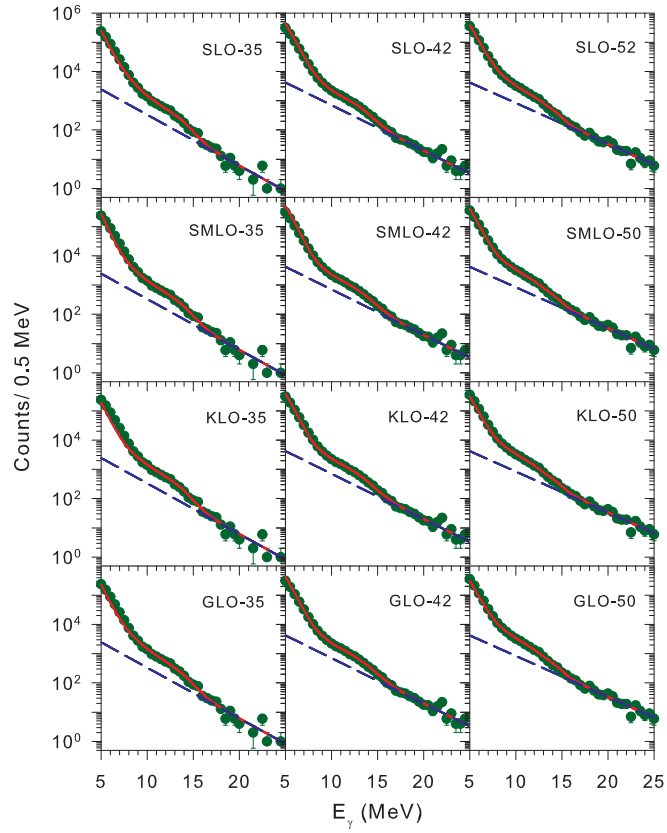

FIG. 3. Experimental high-energy γ-ray spectra (symbols) originated from the decay of ^{201}Tl compound nucleus along with the results (lines) of statistical model calculations with different PSF models. The dashed lines represent the bremsstrahlung component.

expressed as $\tilde{a} = \alpha A + \beta A^{2/3}$. The global values of α, β, and γ_1 for the BFM and CTM can be found in Table 4.3 of TALYS-1.95 manual as well as Ref. [54]. It should be emphasized that the γ-decay rate is influenced by both the strength function and level density prescriptions. Since we are exploring the various strength function models, the same level density prescription is utilized for a given reaction. The default values of the level density parameters, as implemented in the TALYS code, were employed. To fit the high-energy γ-ray spectra, the GDR parameters were adjusted in different strength function models, as previously mentioned.

IV. RESULTS AND DISCUSSIONS

In Figs. 2 and 3, measured high-energy γ-ray spectra are shown for ^{62}Zn and ^{201}Tl, respectively, along with the results of the statistical model calculations. The γ rays above $E_\gamma \gtrapprox 10$ MeV originate primarily from the initial stages of the decay cascade in competition with particle evaporation, while those below $E_\gamma \lessapprox 10$ MeV, are produced from the decay below the particle emission threshold. There is some contribution of bremsstrahlung γ rays, which is parametrized by $\sigma = \sigma_0 \exp(-E_\gamma/E_0)$. These bremsstrahlung γ rays originate from the nucleon-nucleon, especially, the neutron-proton interactions in the initial stages of the reaction [55,56]. The parameters σ_0 and E_0 were selected to fit the region of the spectrum dominated by the bremsstrahlung, e.g., for ^{201}Tl, the bremsstrahlung fit was done for γ rays above $E_\gamma \approx 18$ MeV, whereas, for ^{62}Zn, the fit was done above $E_\gamma \approx 22$ MeV. For a given reaction at a given beam energy, the same bremsstrahlung parameters were utilized while using different strength function models. The calculated γ-ray spectra were convoluted with the response function of the LAMBDA spectrometer, simulated using the GEANT3 toolkit, before comparing with the experimental spectra. It is important to highlight that, with the default parameters of the NLD as implemented in the TALYS code, the BFM prescription was found to be appropriate for ^{62}Zn, whereas for ^{201}Tl, the CTM was more suitable. In general, for a given PSF, the CTM predicts a lower yield of high-energy γ rays compared to that obtained with the BFM. It happens because the value of $\tilde{a}$ is large in the CTM which results in a steeper increase in level density

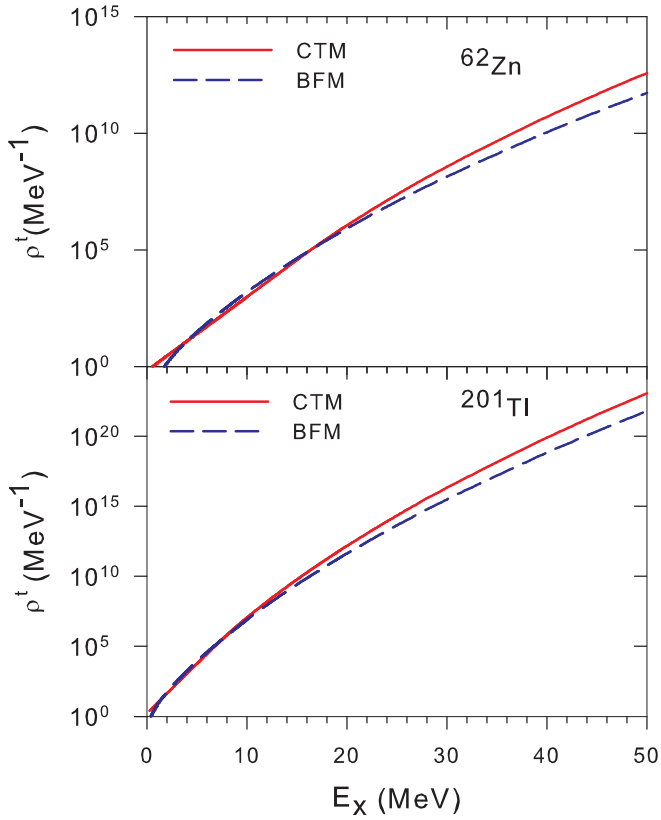

FIG. 4. Total level densities as a function of excitation energy for ^{62}Zn (upper panel) and ^{201}Tl (lower panel).

as function of excitation energy as shown in Fig. 4. Thus, the value of $\tilde{a}$ determines the shape of the high-energy γ-ray spectrum, which cannot be fully compensated by varying the GDR parameters. For example, using the CTM, the spectrum for ^{62}Zn populated at $E^* = 40.8$ MeV could be reasonably reproduced with an extra strength of ≈40% compared to the TRK limit. However, the spectra at $E^* = 29.5$ MeV could not be described by using the CTM with reasonable variation in the GDR parameters. One potential approach could be to modify the slope of the NLD by adjusting the value of $\tilde{a}$ for the nuclei in the decay cascade. However, instead of an arbitrary variation of $\tilde{a}$, we have employed BFM with default values of the level density parameters which are determined from the best description of level densities over a wide range of nuclei [54]. A similar discussion holds for ^{201}Tl for which the CTM was found to be preferable. Interestingly, as can be seen from Table II, the high-energy spectra originating from the decay of the same initial CN populated at different excitation energies could be described by the same value of $\tilde{a}$.

Figures 5 and 6 present the divided spectra for ^{62}Zn and ^{201}Tl, respectively, where the symbols (line) are obtained by point-wise division of the experimental (calculated) high-energy γ-ray spectrum with the results of a statistical model calculation performed using a constant dipole strength instead of the GDR strength. The effects of the variation of the GDR parameters are more discernible in the divided spectra compared to the high-energy spectra. In Table II, the deduced GDR parameters which were obtained by using different PSF are shown along with other relevant parameters. For a given reaction at a given beam energy, different PSF models put forward approximately the same energy (within ≈ 1 MeV) and strength of the GDR. However, relatively large variations were observed in the predicted GDR widths by different PSF models. It is also interesting to note that the data for ^{62}Zn at both excitation energies could be reproduced using the same

TABLE II. Different model parameters utilized in the analysis and deduced from the measured data.

CN	E^* MeV	$< J >$ $\hbar$	T MeV	E_0 MeV	$\tilde{a}$ MeV^{-1}	PSF Model	E_G MeV	S_G	Γ_G MeV	$\Gamma(T)$ MeV
^{62}Zn	29.5	12.4 ± 3.9	0.9 ± 0.4	5.0 ± 0.2	7.54	SLO	17.1 ± 0.2	1.00 ± 0.03	6.7±0.3	6.7 ± 0.3
						SMLO	17.6 ± 0.2	0.90 ± 0.03	6.5±0.3	7.2 ± 0.7
						KLO	17.5 ± 0.2	1.00 ± 0.03	7.1±0.4	7.9 ± 0.8
						GLO	16.9 ± 0.2	1.00 ± 0.03	7.1±0.3	5.5 ± 0.6
	40.8	13.6 ± 4.1	1.5 ± 0.2	5.2 ± 0.2	7.54	SLO	16.4 ± 0.2	1.17 ± 0.02	7.0±0.3	7.0 ± 0.3
						SMLO	17.1 ± 0.2	1.19 ± 0.02	6.5 ± 0.3	8.6 ± 0.7
						KLO	17.2 ± 0.2	1.00 ± 0.03	7.1±0.3	9.4 ± 0.7
						GLO	16.2 ± 0.2	1.00 ± 0.03	7.1±0.3	6.6 ± 0.7
^{201}Tl	32.8	16.9 ± 6.1	0.92 ± 0.04	2.5 ± 0.2	23.62	SLO	14.5 ± 0.3	0.98 ± 0.06	3.6 ± 0.5	3.6 ± 0.5
						SMLO	14.4 ± 0.3	1.00 ± 0.06	3.8 ± 0.4	4.4 ± 0.5
						KLO	14.8 ± 0.3	1.02 ± 0.05	4.5 ± 0.5	5.2 ± 0.6
						GLO	14.7 ± 0.3	1.00 ± 0.06	4.8 ± 0.5	3.9 ± 0.6
	39.6	19.0 ± 6.5	1.08 ± 0.03	2.8 ± 0.2	23.62	SLO	14.0 ± 0.2	1.06 ± 0.06	3.8 ± 0.3	3.8 ± 0.3
						SMLO	14.4 ± 0.2	1.00 ± 0.04	4.0 ± 0.3	4.9 ± 0.4
						KLO	14.5 ± 0.2	0.97 ± 0.04	4.8 ± 0.3	5.9 ± 0.4
						GLO	14.3 ± 0.2	1.00 ± 0.04	4.8 ± 0.3	4.1 ± 0.4
	47.5	21.1 ± 6.7	1.24 ± 0.03	3.1 ± 0.2	23.62	SLO	13.1 ± 0.2	1.00 ± 0.04	4.5 ± 0.4	4.5 ± 0.4
						SMLO	13.1 ± 0.2	1.00 ± 0.03	4.3 ± 0.3	5.8 ± 0.4
						KLO	13.5 ± 0.2	1.00 ± 0.04	5.5 ± 0.3	7.4 ± 0.4
						GLO	12.8 ± 0.2	1.00 ± 0.04	5.2 ± 0.3	4.9 ± 0.4

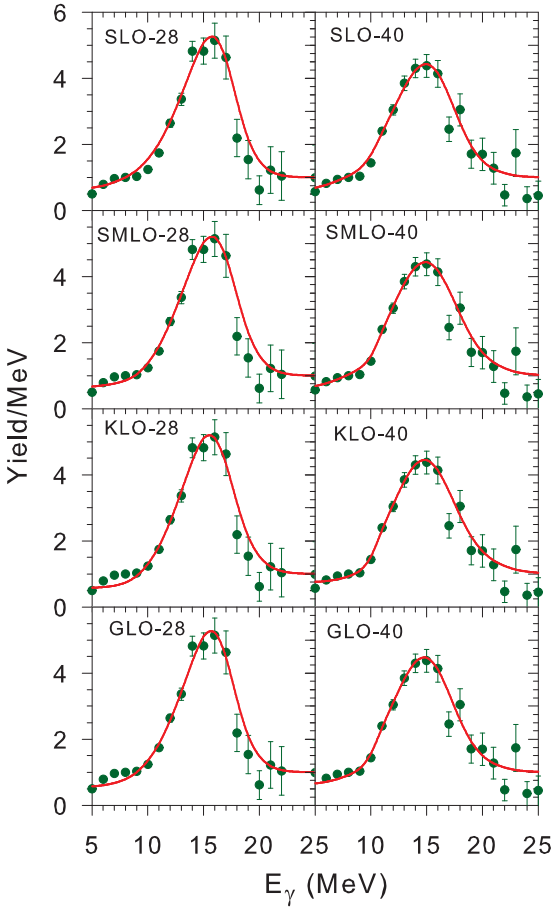

FIG. 5. Experimental (symbols) and best-fit (lines) divided spectra for ^{62}Zn.

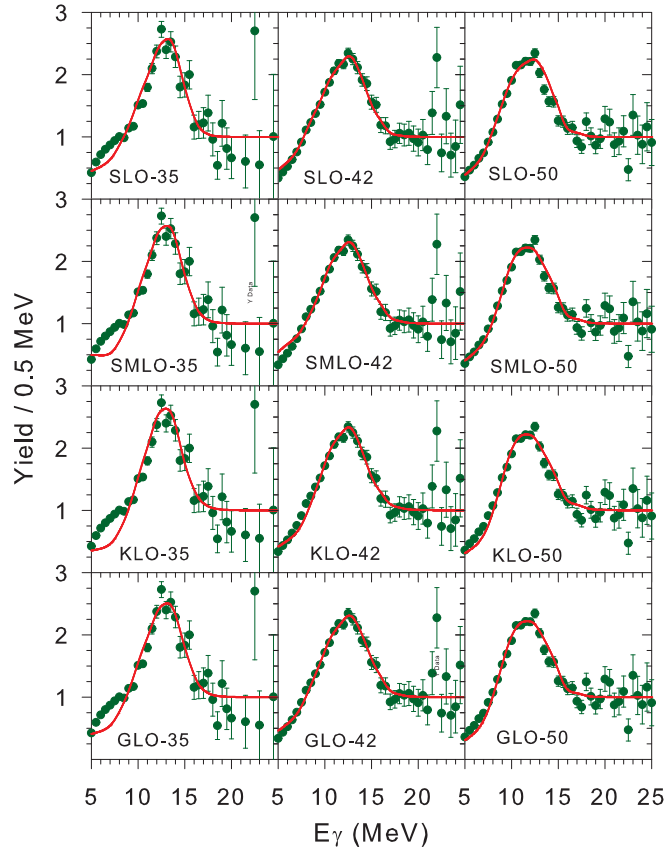

FIG. 6. Experimental (symbols) and best-fit (lines) divided spectra for ^{201}Tl.

value of Γ_G for a given temperature-dependent PSF model. In contrast, for ^{201}Tl, different values of Γ_G are required, for a given PSF model, to fit the data at different excitation energies.

It is intriguing to note that, although the data could be reasonably reproduced for both the nuclei by all PSF models, the extracted values of the GDR parameters, especially the width, are different. It occurs because at each step along the decay cascade, the values of the strength function is different for different models. In Fig. 7, the PSFs for different models are presented, as an example, for ^{201}Tl at $T = 1.08$ MeV corresponding to $E^* = 39.6$ MeV, along with the absorption cross section in the inverse channel. These plots are generated by using the GDR parameters obtained from fitting the high-energy γ-ray spectrum with the respective PSF models. The temperature is calculated using the relation $T = \sqrt{U/a(U)}$, where $U = E^* - E_G - E_{rot} - \Delta$, where the rotational energy of the hot nucleus is given by $E_{rot} = \frac{<J>(<J>+1)\hbar^2}{2I}$, I being the rigid-body moment of inertia and $< J >$ is the average angular momentum of the CN. Δ is the pairing shift as used in the level density prescriptions, and E_G is the average of the GDR energies obtained from different PSF models at a given excitation energy. In Fig. 8 the GDR widths at finite temperature, defined as $\Gamma(T) \equiv \Gamma(E_\gamma = E_G, T)$ are plotted as

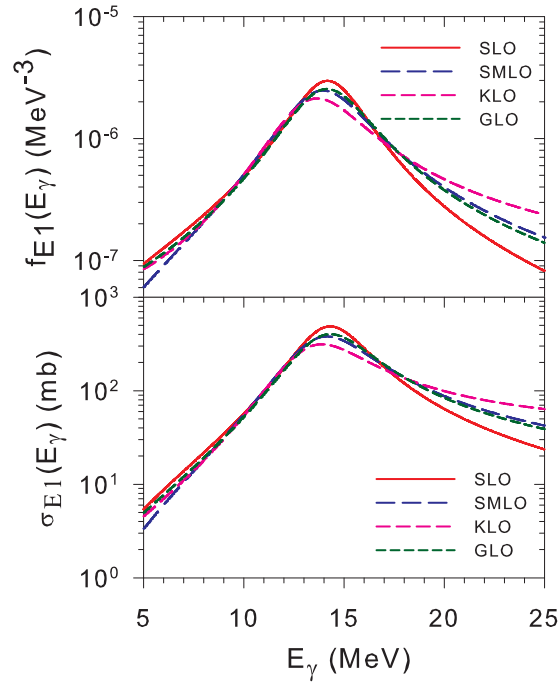

FIG. 7. (Upper panel) Different PSF models used to fit the data of ^{201}Tl at $T = 1.08$ MeV. (Lower panel) Corresponding absorption cross sections in the inverse channel.

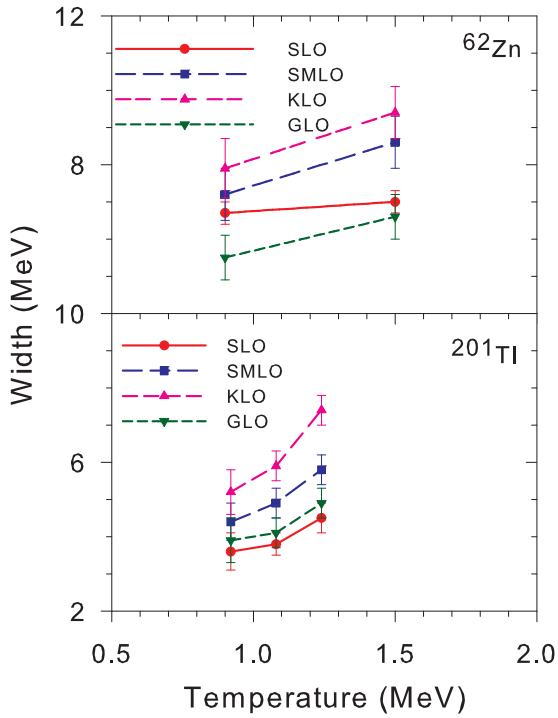

FIG. 8. The GDR widths, determined by using different PSF models, are plotted as a function of temperature for ^{62}Zn (upper panel) and ^{201}Tl (lower panel).

a function of T. The values of $\Gamma(T)$ are deduced using the relations described in Table I with the best-fit values of E_G and Γ_G determined from the experimental data. It is crucial to note that, at a given temperature, the widths obtained using the different PSF models vary approximately by 2–3 MeV. In addition, the variation patterns with temperature are different, especially for ^{201}Tl. Thus, the GDR widths at finite temperatures depend entirely on the PSF model used in the statistical model calculations. In this context it worth mentioning that in Ref. [28] the width of the GDR built on the ground state of the nucleus has been determined by fitting the experimental photoabsorption cross section with the SLO as well as SMLO. Both models put forward approximately the same width. However, as observed in the present study, the widths of the GDR built on the excited states of the nuclei differ for various PSF models at finite temperatures.

Several models have been proposed earlier to explain the variation of the GDR width with temperature. The thermal shape fluctuation model (TSFM) [57–59] calculates the GDR lineshape at finite temperature by taking the weighted average of the lineshapes corresponding to different nuclear deformations. However, it tends to overestimate measured widths at $T \lessapprox 2$ MeV. Notably, the microscopic phonon damping model (PDM) [60,61] and the critical temperature included fluctuation model (CTFM) [13] describe the temperature variation of the GDR width reasonably well. Within the PDM, the width at finite temperature emerges from coupling of the GDR state with particle-hole (ph), particle-particle (pp), and hole-hole (hh) configurations. Within the CTFM, the width remains constant up to a mass-dependent critical temperature and increases thereafter. These insights are drawn primarily from GDR widths determined by using the SLO strength function. However, as observed in the present study, the PSF model dependence of the deduced widths should be taken into account. Additionally, as mentioned earlier, the SMLO describes the γ-ray spectra for ^{62}Zn at both the excitation energies with an identical ground-state width. However, for fitting the measured spectra for ^{201}Tl different ground-state widths were required. Similar observations hold for the KLO and GLO models with the caveat that the required ground state widths were a bit higher, especially for ^{201}Tl. This suggests that the underlying mechanism of the increase in the width in light mass systems could be explained within the temperature-sensitive strength function models. On the other hand, other mechanisms might have significant influence for heavy mass systems. However, more systems should be studied with these modified strength function models before drawing any definite conclusion. It will also be interesting in the future to study isospin mixing, nuclear dissipation, etc., which were studied earlier in hot nuclei using the SLO model strength function, using the temperature-dependent PSF models.

V. SUMMARY AND CONCLUSION

To summarize, we have investigated four different phenomenological photon strength function models in their application to determine the properties of the GDR built on the excited states of both light and heavy mass nuclei. All the models corroborate the measured high-energy γ-ray spectra reasonably well. The variation in the peak energy of the GDR remains within $\approx$1 MeV for different PSF models. However, a large variation is observed in the predicted GDR width at finite temperatures. This observation may significantly influence the theoretical models which perform calculations of the GDR width at finite temperature. The temperature-sensitive strength function models could illuminate new insights into the diverse properties studied in excited nuclei using the GDR as a probe.

ACKNOWLEDGMENTS

The authors acknowledge the contribution of the VECC cyclotron staff for smooth running of the accelerator during the experiment. D.M. acknowledges the valuable email communications with Prof. A. Koning.

[1] M. N. Harakeh and A. van der Woude, *Giant Resonances: Fundamental High-Frequency Mode of Nuclear Excitation* (Clarendon Press, Oxford, 2001).
[2] B. L. Berman and S. C. Fultz, Rev. Mod. Phys. **47**, 713 (1975).
[3] S. S. Dietrich and B. L. Berman, At. Data Nucl. Data Tables **38**, 199 (1988).
[4] K. A. Snover, Annu. Rev. Nucl. Part. Sci. **36**, 545 (1986), and references therein.

[5] J. J. Gaardhøje, Annu. Rev. Nucl. Part. Sci. **42**, 483 (1992), and references therein.
[6] A. Schiller *et al.*, At. Data Nucl. Data Tables **93**, 549 (2007), and references therein.
[7] D. R. Chakrabarty *et al.*, Eur. Phys. J. A **52**, 143 (2016), and references therein.
[8] D. Santonocito *et al.*, Eur. Phys. J. A **56**, 279 (2020), and references therein.
[9] J. O. Newton, B. Herskind, R. M. Diamond, E. L. Dines, J. E. Draper, K. H. Lindenberger, C. Schuck, S. Shih, and F. S. Stephens, Phys. Rev. Lett. **46**, 1383 (1981).
[10] D. R. Chakrabarty, M. Thoennessen, N. Alamanos, P. Paul, and S. Sen, Phys. Rev. Lett. **58**, 1092 (1987).
[11] O. Wieland *et al.*, Phys. Rev. Lett. **97**, 012501 (2006).
[12] S. Mukhopadhyay *et al.*, Phys. Lett. B **709**, 9 (2012).
[13] D. Pandit *et al.*, Phys. Lett. B **713**, 434 (2012).
[14] B. Dey *et al.*, Phys. Lett. B **731**, 92 (2014).
[15] M. Ciemala *et al.*, Phys. Rev. C **91**, 054313 (2015).
[16] D. Mondal *et al.*, Phys. Lett. B **784**, 423 (2018).
[17] P. Heckman *et al.*, Phys. Lett. B **555**, 43 (2003).
[18] F. Pühlhofer, Nucl. Phys. A **280**, 267 (1977).
[19] D. M. Brink, Some aspects of the interactions of fields with matter, Ph.D. thesis, University of Oxford, 1955.
[20] P. Axel, Phys. Rev. **126**, 671 (1962).
[21] M. Guttormsen, A. C. Larsen, A. Gorgen, T. Renstrom, S. Siem, T. G. Tornyi, and G. M. Tveten, Phys. Rev. Lett. **116**, 012502 (2016).
[22] D. Martin *et al.*, Phys. Rev. Lett. **119**, 182503 (2017).
[23] M. Markova *et al.*, Phys. Rev. Lett. **127**, 182501 (2021).
[24] C. T. Angell, S. L. Hammond, H. J. Karwowski, J. H. Kelley, M. Krticka, E. Kwan, A. Makinaga, and G. Rusev, Phys. Rev. C **86**, 051302(R) (2012).
[25] J. Isaak *et al.*, Phys. Lett. B **788**, 225 (2019).
[26] D. R. Chakrabarty, S. Sen, M. Thoennessen, N. Alamanos, P. Paul, R. Schicker, J. Stachel, and J. J. Gaardhoje, Phys. Rev. C **36**, 1886 (1987).
[27] P. Heckman *et al.*, Nucl. Phys. A **750**, 175 (2005).
[28] V. A. Plujko *et al.*, At. Data Nucl. Data Tables **123–124**, 1 (2018).
[29] M. Guttormsen *et al.*, Nucl. Instrum. Methods Phys. Res. A **255**, 518 (1987).
[30] A. Schiller *et al.*, Nucl. Instrum. Methods Phys. Res. A **447**, 498 (2000).
[31] M. Markova *et al.*, Phys. Rev. C **108**, 014315 (2023).
[32] I. K. B. Kullmann *et al.*, Phys. Rev. C **99**, 065806 (2019).
[33] L. Crespo Campo *et al.*, Phys. Rev. C **94**, 044321 (2016).
[34] Oslo database [https://www.mn.uio.no/fysikk/english/research/about/infrastructure/OCL/nuclear-physics-research/compilation/].
[35] J. Kopecky and M. Uhl, Phys. Rev. C **41**, 1941 (1990).
[36] S. Goriely, Phys. Lett. B **436**, 10 (1998).
[37] S. Goriely *et al.*, Eur. Phys. J. A **55**, 172 (2019).
[38] S. Goriely and V. Plujko, Phys. Rev. C **99**, 014303 (2019).
[39] S. Kadmenskij *et al.*, Sov. J. Nucl. Phys. **37**, 165 (1983).
[40] M. N. Harakeh *et al.*, Phys. Lett. B **176**, 297 (1986).
[41] J. A. Behr, K. A. Snover, C. A. Gossett, M. Kicinska-Habior, J. H. Gundlach, Z. M. Drebi, M. S. Kaplan, and D. P. Wells, Phys. Rev. Lett. **70**, 3201 (1993).
[42] D. Mondal *et al.*, Phys. Lett. B **763**, 422 (2016).
[43] G. Gosta *et al.*, Phys. Rev. C **103**, L041302 (2021), and references therein.
[44] N. Dinh Dang, Phys. Rev. C **84**, 034309 (2011).
[45] D. Mondal *et al.*, Phys. Rev. Lett. **118**, 192501 (2017).
[46] M. Thoennessen, D. R. Chakrabarty, M. G. Herman, R. Butsch, and P. Paul, Phys. Rev. Lett. **59**, 2860 (1987).
[47] P. Paul and M. Thoennessen, Annu. Rev. Nucl. Part. Sci. **44**, 65 (1994).
[48] I. Diószegi, N. P. Shaw, A. Bracco, F. Camera, S. Tettoni, M. Mattiuzzi, and P. Paul, Phys. Rev. C **63**, 014611 (2000).
[49] S. Mukhopadhyay *et al.*, Nucl. Instrum. Methods Phys. Res. A **582**, 603 (2007).
[50] D. Pandit *et al.*, Nucl. Instrum. Methods Phys. Res. A **624**, 148 (2010).
[51] A. Koning *et al.*, Eur. Phys. J. A **59**, 131 (2023).
[52] A. Gilbert and A. G. W. Cameron, Can. J. Phys. **43**, 1446 (1965).
[53] A. V. Ignatyuk *et al.*, Sov. J. Nucl. Phys. **21**, 255 (1975), Yad. Fiz. **21**, 485 (1975).
[54] A. J. koning *et al.*, Nucl. Phys. A **810**, 13 (2008).
[55] W. Cassing *et al.*, Phys. Rep. **188**, 363 (1990).
[56] H. Nifenecker and J. A. Pinston, Annu. Rev. Nucl. Part. Sci. **40**, 113 (1990).
[57] Y. Alhassid, B. Bush, and S. Levit, Phys. Rev. Lett. **61**, 1926 (1988).
[58] W. E. Ormand, P. F. Bortignon, and R. A. Broglia, Phys. Rev. Lett. **77**, 607 (1996).
[59] D. Kusnezov, Y. Alhassid, and K. A. Snover, Phys. Rev. Lett. **81**, 542 (1998).
[60] N. D. Dang and A. Arima, Phys. Rev. Lett. **80**, 4145 (1998).
[61] N. D. Dang and A. Arima, Nucl. Phys. A **636**, 427 (1998).